Self-interaction-free time-dependent density-functional theory for molecular processes in strong fields: High-order harmonic generation of H$_2$ in intense laser fields

Xi Chu and Shih-I Chu

Department of Chemistry, University of Kansas, and Kansas Center for Advanced Scientific Computing, Lawrence, Kansas 66045
(Received 5 June 2000; published 17 January 2001)

We present a *self-interaction-free* time-dependent density-functional theory (TDDFT) for nonperturbative treatment of multiphoton processes of many-electron molecular systems in intense laser fields. The time-dependent exchange-correlation (xc) energy potential with proper short- and long-range potential is constructed by means of the *time-dependent optimized effective potential* (OEP) method and the incorporation of an explicit *self-interaction-correction* (SIC) term. The resulting time-dependent OEP/SIC equations are structurally similar to the time-dependent Hartree-Fock equations, but include the many-body effects through an orbital-*independent* single-particle *local* time-dependent xc potential. A numerical time-propagation technique is introduced for accurate and efficient solution of the TDDFT/OEP-SIC equations for two-center diatomic molecular systems. This procedure involves the use of a *generalized pseudospectral* method for *nonuniform* optimal grid discretization of the Hamiltonian in prolate spheroidal coordinates and a split-operator scheme in the *energy* representation for the time development of the electron orbital wave functions. High-precision time-dependent wave functions can be obtained by this procedure with the use of only a modest number of spatial grid points. The theory is applied to a detailed study of high-order harmonic generation (HHG) processes of H$_2$ molecules in intense pulsed laser fields. Particular attention is paid to the exploration of the spectral and temporal structures of HHG by means of the wavelet time-frequency analysis. The results reveal striking details of the spectral and temporal fine structures of HHG, providing new insights regarding the detailed HHG mechanisms in different energy regimes.

I. INTRODUCTION

The study of multiphoton and nonlinear optical processes of atoms and molecules in intense laser fields is a subject of much current interest in science and technology. To describe such strong-field processes using *ab initio* wave-function approach, it is necessary to solve the time-dependent Schrödinger equation of many-electron systems, which is far beyond the capability of current computational technology. In this paper we present a nonperturbative formalism based on the extension of the time- dependent density-functional theory (TDDFT) for the study of many-electron molecular systems in strong fields.

Since the fundamental work of Hohenberg and Kohn [1] and Kohn and Sham [2], the (steady-state) density-functional theory (DFT) has become a widely used formalism for electronic structure calculations of the ground-state properties of atoms, molecules, and solids [3–7]. In the Kohn-Sham DFT formalism, the electron density is decomposed into a set of orbitals, leading to a set of one-electron Schrödinger-like equations to be solved self-consistently. DFT is computationally much less expensive than the traditional *ab initio* many-electron wave-function approaches and this accounts for its great success for large systems. However, the DFT is well developed mainly for the ground-state properties only. The treatment of excited and resonance states structure and time-dependent processes, both essential to the quantitative study of multiphoton dynamics of many-electron systems, within the density-functional theory, is much less developed.

The central theme of the modern TDDFT [8–14] is a set of time-dependent Kohn-Sham equations which are structur-ally similar to the time-dependent Hartree-Fock equations but include in principle exactly all many-body effects through a local time-dependent exchange-correlation (xc) potential. With the exception of several recent works [11–13], previous applications of the TDDFT fall in the regime of linear or nonlinear response in weak fields for which the perturbation theory is [8–10] applicable. Recently, an alternative nonperturbative formulation of the time-dependent DFT [15] and time-dependent current DFT [16] based on the extension of the *generalized Floquet formalism* [17] has been introduced, allowing exact transformation of the time-dependent Kohn-Sham-like equations into an equivalent *time-independent* non-Hermitian Floquet matrix eigenvalue problem. Such a TDDFT-Floquet formalism provides a general *time-independent* approach for nonperturbative treatment of multiphoton processes of many-electron quantum systems in the presence of *periodic, quasiperiodic, or multi-color* laser fields. In this paper we focus on the time-dependent approach and extend the TDDFT with *optimized effective potential* (OEP) and *self-interaction-correction* (SIC) recently developed [12,13] for the atomic systems in arbitrarily time-dependent fields to the molecular systems.

In actual DFT or TDDFT calculations, one needs to input the xc-energy functionals whose exact forms are not known. It is known [3] that the xc energy functionals commonly used such as the *local spin density approximation* (LSDA) [3,18] or the more refined *generalized gradient approximation* (GGA) [3,19–21], suffer a severe deficiency, namely, the corresponding xc potentials do not possess the correct long-range ($-1/r$) behavior. As such, while the total energies of the ground states of atoms and molecules predicted by these explicit xc density functionals are rather accurate,

the ionization potentials obtained from the highest occupied orbital energies are less satisfactory [3], typically 30–40% too low. Such a problem can be attributed to the existence of *self-interaction energy* in the conventional DFT formalism using LSDA or GGA. For accurate treatment of photoionization or multiphoton ionization processes, it is necessary that both the ionization potentials and the excited state properties be described more properly.

In a recent paper, we have presented an extension of the DFT for more accurate treatment of both the ionization potentials of the ground states as well as the photoabsorption spectrum of autoionizing resonances [22]. The results are in good agreement with available experimental data well within a few percents [22]. The method is based on the extension of the KLI (Krieger- Li-Iafrate)'s semianalytical treatment [23] of the OEP formalism [24,25] along with the use of an explicit SIC form [26]. As shown in our recent work [22], the optimized effective potential so constructed has the proper long-range ($-1/r$) behavior and is capable of providing high accuracy for both excited and autoionizing resonance states. In a recent paper, we extend the OEP/KLI-SIC formalism for the atomic systems to the time domain [12]. We note that a related time-dependent OEP/KLI formalism has been developed by Ullrich *et al.*, [11] in the exchange (x)-only limit. In the latter approach [11], the *non-local* Hartree-Fock exchange functional form is used instead of the explicit SIC form [12] in the construction of the optimized effective potential. As shown in our recent works for atomic systems [12,13], the use of explicit SIC form in the time-dependent OEP/KLI calculations involves only orbital-*independent* single-particle *local* potentials for each time step and is thus computationally more efficient and yet the wave functions maintain high accuracy.

The organization of this paper is as follows. First we briefly review the time-dependent DFT formalism with OEP/KLI-SIC in Sec. II for the general treatment of multiphoton dynamics of many-electron atomic and molecular systems in the presence of intense laser fields, taking into account electron correlation and proper long-range behavior of the optimized effective potential. Second, we present a *generalized pseudospectral* (GPS) method in Sec. III for the *nonuniform* optimal spatial discretization of two-center diatomic molecular systems. Third, we outline in Sec. IV a *generalized pseudospectral time-dependent* method for efficient and accurate treatment of the time-dependent OEP/KLI-SIC equations in space and time. And finally in Sec. V we apply the TDDFT/OEP-SIC formalism to a nonperturbative study of *multiple high-order harmonic generation* (HHG) of H_2 molecules in intense pulsed laser fields. Particular attention is paid to the exploration of the fine structures of spectral and time profiles of HHG, providing detailed new physical insights regarding the underlying mechanisms for harmonic generation in different energy regimes.

II. TDDFT WITH OEP-SIC FOR INTENSE-FIELD MULTIPHOTON PROCESSES

In this section we briefly describe the TDDFT with OEP and SIC for multiphoton processes of many-electron systems in intense laser fields. The general formalism is applicable to both atomic and molecular systems. The spin orbitals satisfy the one-electron Schrödinger-like equation, in atomic units,

$$i\frac{\partial}{\partial t}\psi_{i\sigma}(\mathbf{r},t) = \hat{H}(\mathbf{r},t)\psi_{i\sigma}(\mathbf{r},t)$$

$$= \left[-\frac{1}{2}\nabla^2 + v_{eff,\sigma}(\mathbf{r},t) \right]\psi_{i\sigma}(\mathbf{r},t),$$

$$i = 1,2,\ldots,N_\sigma, \quad (1)$$

where $v_{eff,\sigma}(\mathbf{r},t)$ is the time-dependent effective potential depending upon the total electron density $\rho(t)$ and σ is the spin index. The total number of electrons in the system is $N = \Sigma_\sigma N_\sigma$, where $N_\sigma (= N_\uparrow$ or $N_\downarrow)$ is the total number of electrons for a given spin σ. Within the single determinant approximation, the total N-electron wave function can be expressed as

$$\Psi(t) = \frac{1}{\sqrt{N!}}\det[\psi_1 \cdot \psi_2 \ldots \psi_N], \quad (2)$$

and the total electron density at time t is determined by the single-electron orbital wave functions $\{\psi_{i\sigma}\}$ as

$$\rho(\mathbf{r},t) = \sum_\sigma \sum_{i=1}^{N_\sigma} \rho_{i\sigma}(\mathbf{r},t) = \rho_\uparrow(\mathbf{r},t) + \rho_\downarrow(\mathbf{r},t), \quad (3)$$

where $\rho_{i\sigma}(\mathbf{r},t) = \psi_{i\sigma}^*(\mathbf{r},t)\psi_{i\sigma}(\mathbf{r},t)$. The effective potential $v_{eff,\sigma}(\mathbf{r},t)$ in Eq. (1) will be the time-dependent OEP if we choose the set of spin orbitals $\{\psi_{i\sigma}(\mathbf{r},t)\}$ which render the total action functional $A[\{\psi_{i\sigma}(\mathbf{r},t)\}]$ *stationary* [11–13]:

$$\frac{\delta A[\{\psi_{i\sigma}(\mathbf{r},t)\}]}{\delta V_{eff,\sigma}^{OEP}(\mathbf{r},t)} = 0. \quad (4)$$

An essential step is that we propose the following explicit SIC expression for the exchange-correlation (xc) action functional [12,13],

$$A_{xc}[\{\psi_{i\sigma}\}] = \int_{-\infty}^{t_1} dt E_{xc}[\rho_\uparrow(\mathbf{r},t),\rho_\downarrow(\mathbf{r},t)]$$

$$- \sum_\sigma \sum_{i=1}^{N_\sigma} \int_{-\infty}^{t_1} dt\{J[\rho_{i\sigma}] + E_{xc}[\rho_{i\sigma},0]\}, \quad (5)$$

where E_{xc} is the time-dependent exchange-correlation energy functional and

$$J[\rho] = \tfrac{1}{2}\int\int \frac{\rho(\mathbf{r},t)\rho(\mathbf{r}',t)}{|\mathbf{r}-\mathbf{r}'|}d\mathbf{r}d\mathbf{r}'. \quad (6)$$

The use of the SIC form in Eq. (5) removes the spurious self-interaction terms in conventional DFT/TDDFT and results in proper *long-range* potential. Another major advantage of this procedure is that only *local* potential is required

to construct the *orbital-independent* OEP for each time step. This facilitates the numerical computation considerably.

By extending the steady-state OEP/KLI-SIC procedure to the time-dependent case, we obtain the time-dependent OEP as [11–13]:

$$V_{eff,\sigma}^{OEP}(\mathbf{r},t) = v_{ext}(\mathbf{r},t) + \frac{\delta J[\rho]}{\delta\rho_\sigma(\mathbf{r},t)} + V_{SIC,\sigma}(\mathbf{r},t). \quad (7)$$

Here $v_{ext}(\mathbf{r},t)$ is the "external" potential due to the interaction of the electron with the external laser field and the the nuclei, and

$$V_{SIC,\sigma}(\mathbf{r},t) = \sum_i \frac{\rho_{i\sigma}(\mathbf{r},t)}{\rho_\sigma(\mathbf{r},t)}\{v_{i\sigma}(\mathbf{r},t) + [\bar{V}_{SIC,\sigma}^i(t) - \bar{v}_{i\sigma}(t)]\}, \quad (8)$$

$$v_{i\sigma}(\mathbf{r},t) = \frac{\delta E_{xc}[\rho_\uparrow(\mathbf{r},t),\rho_\downarrow(\mathbf{r},t)]}{\delta\rho_\sigma(\mathbf{r},t)} - \frac{\delta J[\rho_{i\sigma}(\mathbf{r},t)]}{\delta\rho_{i\sigma}(\mathbf{r},t)}$$
$$- \frac{\delta E_{xc}[\rho_{i\sigma}(\mathbf{r},t),0]}{\delta\rho_{i\sigma}(\mathbf{r},t)}, \quad (9)$$

and

$$\bar{V}_{SIC,\sigma}^i(t) = \langle\psi_{i\sigma}|V_{SIC,\sigma}(\mathbf{r},t)|\psi_{i\sigma}\rangle, \quad (10)$$

$$\bar{v}_{i\sigma}(t) = \langle\psi_{i\sigma}|v_{i\sigma}(\mathbf{r},t)|\psi_{i\sigma}\rangle. \quad (11)$$

In Eqs. (10) and (11), $\bar{V}_{SIC,\sigma}^i$ and $\bar{v}_{i\sigma}$ are constants at a given time t, although the value of $\bar{V}_{SIC,\sigma}^i$ is unknown, The KLI method [11–13,23] suggests a way to calculate $\bar{V}_{SIC,\sigma}^i(t) - \bar{v}_{i\sigma}^i(t)$ through a solution of the following linear equations

$$\sum_{i=1}^{N_\sigma} [\delta_{ji,\sigma} - M_{ji,\sigma}(t)][\bar{V}_{SIC,\sigma}^i(t) - \bar{v}_{i\sigma}(t)] = \bar{V}_{j\sigma}^s(t) - \bar{v}_{j\sigma}(t),$$

$$j = 1,2,\dots,N_\sigma, \quad (12)$$

where

$$M_{ji,\sigma}(t) = \int \frac{\rho_{j\sigma}(\mathbf{r},t)\rho_{i\sigma}(\mathbf{r},t)}{\rho_\sigma(\mathbf{r},t)} d\mathbf{r}, \quad (13)$$

$$\bar{V}_{j\sigma}^s(t) = \langle\psi_{j\sigma}|\sum_{i=1}^{N_\sigma} \frac{\rho_{i\sigma}(\mathbf{r},t)v_{i\sigma}(\mathbf{r},t)}{\rho_\sigma(\mathbf{r},t)}|\psi_{j\sigma}\rangle. \quad (14)$$

In the time-dependent OEP/KLI-SIC method outlined here, Eqs. (1) and (7) are to be solved self-consistently. Note that Eq. (1) is an initial value problem and the initial wave function can be determined by

$$\psi_{i\sigma}(\mathbf{r},t)_{t=0} = \phi_{i\sigma}(\mathbf{r})\cdot e^{-i\epsilon_{i\sigma}t}|_{t=0}, \quad (15)$$

where $\phi_{i\sigma}(\mathbf{r})$ and $\epsilon_{i\sigma}$ are the eigenfunction and eigenvalue of the time-independent Kohn-Sham equation (with OEP/SIC) for the field-free case [22].

The TDDFT/OEP-SIC procedure outlined in this section is general and applicable to any atomic and molecular systems. For the special case of homonuclear diatomic molecules, our present focus, the time-dependent OEP potential, Eq. (7), has the following explicit form:

$$V_{eff,\sigma}^{OEP}(\mathbf{r},t) = -\frac{Z_1}{|\mathbf{R}_1-\mathbf{r}|} - \frac{Z_2}{|\mathbf{R}_2-\mathbf{r}|} + \int d^3r'\frac{\rho(\mathbf{r}',t)}{|\mathbf{r}-\mathbf{r}'|}$$
$$+ \mathbf{E}(t)\cdot\mathbf{r}\sin\omega t + V_{SIC,\sigma}(\mathbf{r},t), \quad (16)$$

where $V_{SIC,\sigma}(\mathbf{r},t)$ is given in Eq. (8). Here $\mathbf{r}$ is the electronic coordinate, $\mathbf{E}(t)$ the electric field amplitude, and $\mathbf{R}_1 = (0,0,a)$ and $\mathbf{R}_2 = (0,0,-a)$ are the coordinates of the two nuclei in Cartesian coordinates, with nuclear charges Z_1 and Z_2, respectively. The internuclear separation R is equal to $2a$.

III. PSEUDOSPECTRAL SPATIAL DISCRETIZATION OF TWO-CENTER SYSTEMS

In this section, we first present the procedure for the spatial discretization and solution of field-free two-center (diatomic molecular) systems. We shall use the prolate spheroidal coordinates (μ,ν,ϕ), $0<\mu<\infty, 0<\nu<\pi, 0<\phi < 2\pi$, for the description of the system:

$$x = a\sinh\mu\sin\nu\cos\phi, \quad (17)$$

$$y = a\sinh\mu\sin\nu\sin\phi, \quad (18)$$

$$z = a\cosh\mu\cos\nu. \quad (19)$$

Due to the axial symmetry of the diatomic systems, the field-free solution takes the form

$$\Psi_m(\mathbf{r}) = e^{im\varphi}\Phi(\mu,\nu), \quad (m=0,\pm1,\pm2,\dots). \quad (20)$$

We first consider the *nonuniform* optimal discretization of the spatial coordinates by means of the GPS technique [27]. In the GPS method, we expand any spatial wave function $\Phi(\mu,\nu)$ by $\Phi_{N_\mu,N_\nu}(\mu,\nu)$, the polynomials of order N_μ and N_ν in μ and ν, respectively,

$$\Phi(\mu,\nu) \simeq \Phi_{N_\mu,N_\nu}(\mu,\nu)$$
$$= \sum_{i=0,j=0}^{N_\mu,N_\nu} \phi(\mu_i,\nu_j)g_i(x(\mu))g_j(y(\nu)), \quad (21)$$

and further require the approximation to be exact at the collocation points, i.e., $\Phi_{N_\mu,N_\nu}(\mu_i,\nu_j) = \phi(\mu_i,\nu_j) \equiv \phi_{ij}$, where $\{x(\mu_i)\}$ and $\{y(\nu_j)\}$ are the two sets of collocation points to be described below. In Eq. (21), $g_i(x)$ and $g_j(y)$ are the cardinal functions [27,28] defined as

$$g_i(x) = -\frac{1}{N_\mu(N_\mu+1)P_{N_\mu}(x_i)}\frac{(1-x^2)P'_{N_\mu}(x)}{x-x_i}, \quad (22)$$

$$g_j(y) = -\frac{1}{N_\nu(N_\nu+1)P_{N_\nu}(y_j)} \frac{(1-y^2)P'_{N_\nu}(y)}{y-y_j}. \quad (23)$$

In the case of the Legendre pseudospectral method [27,28], which we adopt in this article, the boundary points are $x_0 = y_0 = -1$ and $x_{N_\mu} = y_{N_\nu} = 1$. $x_i(i=1,\ldots,N_\mu-1)$ and $y_j(j=1,\ldots,N_\nu-1)$ are the collocation points determined, respectively, by the roots of the first derivative of the Legendre polynomial P_{N_μ} with respect to x and the first derivative of P_{N_ν} with respect to y, namely,

$$P'_{N_\mu}(x_i) = 0, \quad (24)$$

$$P'_{N_\nu}(y_j) = 0. \quad (25)$$

It follows that the cardinal functions possess the following unique properties

$$g_i(x_{i'}) = \delta_{i,i'}, \quad (26)$$

$$g_j(y_{j'}) = \delta_{j,j'}. \quad (27)$$

We shall use the following mapping relationships between μ and x and between ν and y:

$$\mu = L\frac{1+x}{1-x}, \quad (28)$$

$$\nu = \frac{\pi}{2}(1+y), \quad (29)$$

where $x \in [-1,1]$, $y \in [-1,1]$, $\mu \in [0,\infty]$, $\nu \in [0,\pi]$, and L is a mapping parameter. The collocation points of $x(\mu)$ and $y(\nu)$ are determined by Eqs. (24) and (25).

A most detailed discussion of the construction of the differentiation matrix and the symmetrization of the Hamiltonian matrix is given elsewhere [27]. A major advantage of the outlined generalized pseudospectral method is that it allows for *nonuniform* optimal spatial grid discretization: denser mesh near the nuclei and sparser mesh for long-range part of the Coulombic potential. With the use of only a modest number of grid points, high-precision eigenvalues and eigenfunctions can be obtained since the physically most important short-range regime is accurately treated. Figure 1 shows the grid structure for two-center diatomic systems.

IV. GENERALIZED PSEUDOSPECTRAL TIME-PROPAGATION METHOD FOR NUMERICAL SOLUTION OF TIME-DEPENDENT OEP/SIC EQUATIONS

In this section we discuss the numerical procedure for the solution of the set of time-dependent OEP/SIC equations, Eq. (1), for two-center systems. The commonly used procedures for the time propagation of the Schrödinger or TDDFT equation employ *equal-spacing* spatial grid discretization [29–32]. For processes such as HHG [33], accurate time-dependent wave functions are required to achieve conver-
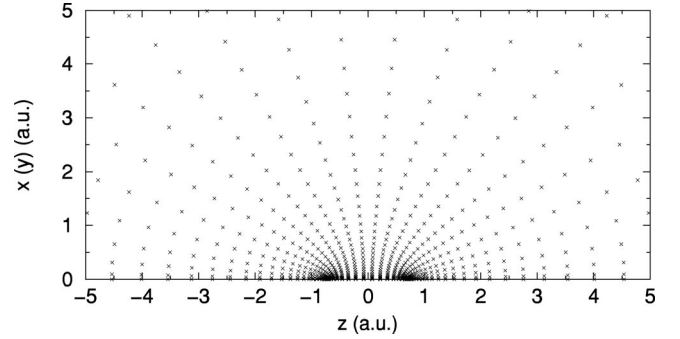

FIG. 1. The grid structure of the spatial coordinates of H_2 obtained by the generalized pseudospectral discretization technique.

gence since the intensity of various harmonic peaks can span a range of many orders of magnitude. High-precision wave functions are generally more difficult to achieve by the equal-spacing spatial-grid-discretization time-dependent techniques, due to the Coulomb singularity at the origin and the long-range behavior of the Coulomb potential. To achieve precision time-dependent wave-function propagation, we have recently introduced a new numerical procedure [34], which consists of the following two basic elements: (i) A GPS technique [27] is used for *nonuniform* optimal grid discretization of the radial coordinates; *denser* mesh near the nucleus and short distances. The extension of the GPS method to the two-center systems has been described in the last section. We have previously shown for the atomic systems that the number of grid points required is orders of magnitude smaller than those used by the equal-spacing discretization methods. Yet higher accuracy in wave functions and therefore HHG spectra can be achieved since the physically more important short-range regime is more accurately treated by this method [34]. (ii) A split-operator technique in the *energy* representation is introduced for efficient time propagation of the wave functions. In the following, we extend this procedure to the numerical solution of the time-dependent OEP/SIC equations in two-center diatomic molecular systems.

Consider the solution of the time-dependent one-electron Kohn-Sham-like equation with OEP/SIC for N-electron systems in linearly polarized laser fields,

$$i\frac{\partial}{\partial t}\psi_{i\sigma}(\mathbf{r},t) = \hat{H}\psi_{i\sigma}(\mathbf{r},t) = [\hat{H}_0(\mathbf{r}) + \hat{V}(\mathbf{r},t)]\psi_{i\sigma}(\mathbf{r},t),$$

$$i = 1,2,\ldots,N_\sigma. \quad (30)$$

Here $\hat{H}_0$ is the time-independent Hamiltonian with OEP/SIC at $t=0$, and $\hat{V}$ includes the electron-laser field interaction and the residual time-dependent OEP/SIC:

$$\hat{H}_0(\mathbf{r}) = -\frac{1}{2a^2}\left\{\frac{1}{(\sinh^2\mu+\sin^2\nu)\sinh\mu}\frac{\partial}{\partial\mu}\left(\sinh\mu\frac{\partial}{\partial\mu}\right)\right.$$
$$\left. + \frac{1}{(\sinh^2\mu+\sin^2\nu)\sin\nu}\frac{\partial}{\partial\nu}\left(\sin\nu\frac{\partial}{\partial\nu}\right)\right\}$$
$$+ V^{OEP}_{SIC,\sigma}(\mathbf{r},0), \quad (31)$$

$$\hat{V}(\mathbf{r},t) = -\mathbf{E}(t) \cdot \mathbf{r} \sin \omega t + V_{SIC,\sigma}^{OEP}(\mathbf{r},t) - V_{SIC,\sigma}^{OEP}(\mathbf{r},0), \tag{32}$$

where $\mathbf{E}(t)$ is the electric field, assumed to be parallel to the internuclear $(\hat{\mathbf{z}})$ axis, and $E(t) = Ff(t)$, where $f(t)$ is the envelope function of the laser pulse. We shall extend the second-order split-operator technique in prolate spheroidal coordinates and in the *energy* representation for the propagation of the time-dependent OEP/SIC equations:

$$\psi_{i\sigma}(\mathbf{r},t+\Delta t) \simeq \exp(-i\hat{V}(\mathbf{r},t)\Delta t/2)\exp(-i\hat{H}_0(\mathbf{r})\Delta t)$$
$$\times \exp(-i\hat{V}(\mathbf{r},t)\Delta t/2)\psi_{i\sigma}(\mathbf{r},t) + O(\Delta t^3). \tag{33}$$

Note that such an expression is different from the conventional split-operator techniques [29–32], where $\hat{H}_0$ is usually chosen to be the kinetic-energy operator and $\hat{V}$ the remaining Hamiltonian depending on the spatial coordinates only. The use of the *energy* representation in Eq. (33) allows the explicit *elimination* of the undesirable fast-oscillating *high-energy* components and speeds up considerably the time propagation [34]. In addition, the symmetry properties possessed by $\hat{H}_0$ can be used to simplify and facilitate the calculations.

To pursue the time propagation, we first discretize the Hamiltonian by the GPS method introduced in the last section. Then the wave function on the pseudospectral grid, $\Psi(\mathbf{r},t)$, is first propagated according to

$$\Psi'(\mathbf{r},t) = e^{-i\hat{V}(\mathbf{r},t)\Delta t/2}\Psi(\mathbf{r},t). \tag{34}$$

Since $\exp(-i\hat{V}(\mathbf{r},t)\Delta t/2)$ is a diagonal matrix in the coordinate representation, this is a fast step as far as the CPU time is concerned. To pursue the next step of propagation in the $\hat{H}_0$ energy space, we construct the time-*independent* evolution operator

$$e^{-i\hat{H}_0\Delta t} \equiv \hat{S}, \tag{35}$$

by means of the GPS discretization and solution of the field-free Hamiltonian, Eq. (31):

$$\hat{H}_0(\mu,\nu)\chi_k(\mu,\nu) = \epsilon_k\chi_k(\mu,\nu). \tag{36}$$

Then the matrix S can be constructed as

$$S_{ij} = \sum_k \chi_k(\mathbf{r}_i)\chi_k^*(\mathbf{r}_j)e^{-i\epsilon_k\Delta t}. \tag{37}$$

Note that S is a complex symmetric matrix and needs to be constructed only once. Thus the time propagation in the energy space,

$$\Psi''(\mathbf{r},t) = \exp(-i\hat{H}_0\Delta t)\Psi'(\mathbf{r},t) = \hat{S}\Psi'(\mathbf{r},t), \tag{38}$$

is reduced to the matrix-vector product $[O(N^2)$ operation] which can be performed efficiently using the basic linear algebra subroutines. Note that since only a modest number of

grid points (N) are required in the present method, and since only half of the grid points in the ν coordinate are required for homonuclear diatomic molecules, the overall operation is rather efficient. Finally we perform another fast propagation step similar to that in Eq. (34):

$$\Psi(\mathbf{r},t+\Delta t) = \exp(-i\hat{V}(\mathbf{r},t)\Delta t/2)\Psi''(\mathbf{r},t). \tag{39}$$

This completes one time propagation step in Eq. (33). After the time-dependent single-electron wave functions $\{\psi_{i\sigma}\}$ are obtained, the total electron density $\rho(t)$ can be determined. The induced dipole moment and dipole acceleration can now be expressed, respectively, as

$$d(t) = \int \rho(\mathbf{r},t)zd^3\mathbf{r} = \sum_{i\sigma} \langle \psi_{i\sigma}(\mathbf{r},t)|z|\psi_{i\sigma}(\mathbf{r},t)\rangle, \tag{40}$$

and

$$d_A(t) = \int \rho(\mathbf{r},t)\frac{d^2z}{dt^2}d^3\mathbf{r}$$
$$= \sum_{i\sigma} \langle \psi_{i\sigma}(\mathbf{r},t)| -\frac{\partial V_{SIC,\sigma}^{OEP}(\mathbf{r},t)}{\partial z}$$
$$+ \frac{\mathbf{E}(t)\cdot\mathbf{r}\sin(\omega t)}{z}|\psi_{i\sigma}(\mathbf{r},t)\rangle. \tag{41}$$

The corresponding HHG power spectrum can now be obtained by the Fourier transformation of the respective time-dependent dipole moment or dipole acceleration:

$$P(\omega) = \left|\frac{1}{t_f-t_i}\int_{t_i}^{t_f}d(t)e^{-i\omega t}\right|^2 = |d(\omega)|^2, \tag{42}$$

and

$$P_A(\omega) = \left|\frac{1}{t_f-t_i}\frac{1}{\omega^2}\int_{t_i}^{t_f}d_A(t)e^{-i\omega t}\right|^2 = |d_A(\omega)|^2. \tag{43}$$

V. HIGH HARMONIC GENERATION OF H_2 IN INTENSE LASER FIELDS: A CASE STUDY

In this section we present an application of the TDDFT/OEP-SIC procedure to the study of HHG of H_2 in intense pulsed laser fields. First we discuss the field-free electronic structure calculations using the steady-state DFT/OEP-SIC procedure [22], and the *generalized pseudospectral* method [27] is extended to discretize the molecular Hamiltonian in the prolate spheroidal coordinates. As a measure of the accuracy of the procedure, we have first tested the method for the H_2^+ molecule, where exact results are available for comparison. Using only a modest number of grid points (20 for the μ coordinate and 9 for the ν coordinate), we obtain the ground-state energy to be -1.1026342144949 a.u., in complete agreement with the exact value of -1.1026342144949 a.u. [35]. For H_2, the calculated ground-state energy is -1.1336 a.u. (using LSDA exchange energy functional only) and -1.1828 a.u. (including both

LSDA exchange and correlation energy functionals), the latter is within 1% of the exact value of $-1.174\,448$ a.u. [36]. If the GGA energy functional such as that of Becke-Lee-Yang-Parr (BLYP) [3] is used, the calculated ground-state energy is improved to $-1.174\,44$ a.u.

In the following we consider the interaction of H_2 molecules with an intense linearly polarized laser fields with wavelength 1064 nm, $\sin^2$ pulse shape, and 20 optical cycles in pulse length. The time-dependent xc potential is constructed by means of the time-dependent OEP/SIC procedure using the LSDA exchange and correlation energy functional for E_{xc} in Eq. (5). We shall assume the electric-field polarization is aligned along the internuclear-axis ($\hat{\mathbf{z}}$) direction. This approximation is justified by the experimental observation that the laser-molecular interaction tends to force the molecule to align along the polarization axis [40,41]. The rotation of the molecules can be also safely ignored under the present short-pulse conditions. In this paper, we shall focus our study on the HHG process of H_2 molecules from the ground vibrational state with the internuclear separation R fixed at the equilibrium distance ($R=R_e=1.4a_0$). The fixed nuclei approximation is justifiable since the zero-point vibration of H_2 in the ground state is rather small (within $0.25a_0$ of R_e) and the inclusion of the vibrational degree of freedom is not expected to alter the main features of the HHG phenomenon, particularly when the time duration of the laser pulse is short. However, the molecular vibration can play a significant role in HHG if the molecule is initially prepared in a highly excited vibrational state. This will be an interesting subject to explore in the future.

The solution of the time-dependent OEP-SIC equation is performed by means of the *time-dependent generalized pseudospectral* method described in Sec. IV. To achieve full convergence for the time propagation, we have used 200 Legendre grid points for the μ coordinate and 40 grid points for the ν coordinate for the time propagation. In the field-free case, the energy and the norm of the wave function is conserved to at least 10 digits of accuracy during the whole time propagation. The time mesh used is about 0.1 a.u. A soft absorber [34] is placed at large electron distance ($r_{max}=60$ a.u.) to filter out the ionized electron wave packet.

Figure 2 shows the time-dependent induced dipole moment and dipole acceleration of H_2 (at $R=R_e=1.4a_0$) for the case of laser intensity $I=10^{14}$ W/cm^2. As a measure of the accuracy of the time-dependent results, Table I and Fig. 3 show the comparison of the HHG power spectrum of H_2 obtained by the Fourier transform of the induced dipole and dipole acceleration, respectively. Excellent agreement of the two spectra is obtained from the lowest harmonics all the way to the cutoff regime, indicating the the full convergence of the time-dependent wave functions.

Figure 4 shows the HHG power spectra of H_2 ($R=1.4$ a.u.) under higher laser intensity $I=3\times10^{14}$ W/cm^2, where the HHG plateau is seen to extend well beyond the 100th order. Again, excellent agreement of the length and acceleration results is obtained. The cutoff harmonics in Figs. 3 and 4 are consistent with the quasiclassical prediction [37–39], namely, $n_{cutoff}\simeq[I_p$
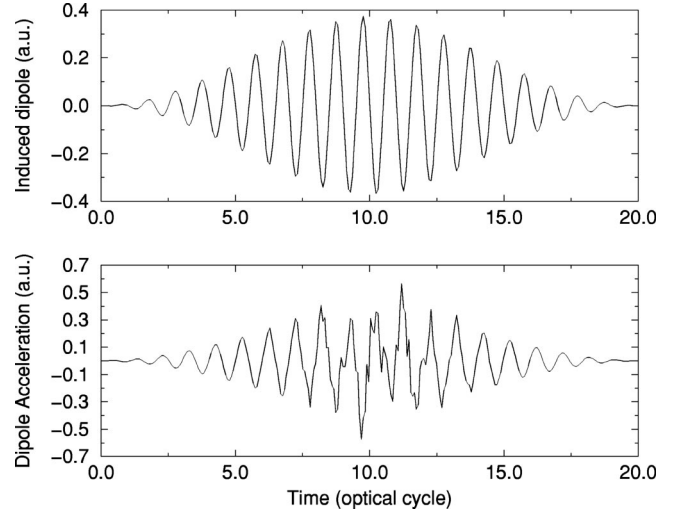

FIG. 2. The induced dipole moment $\langle z(t)\rangle$ and dipole acceleration $\langle (d^2z(t)/dt^2)/\omega_0^2\rangle$ of H_2 at $R=1.4a_0$ as a function of time (in optical cycles). The laser intensity is 10^{14} W/cm^2 and wavelength 1064 nm. The laser field has the $\sin^2$ pulse shape with a pulse duration of 20 optical cycles (o.c.).

$+3.17U_p]/\hbar\omega$, where U_p is the ponderomotive potential. Thus for R near R_e, the behavior of high harmonic generation in H_2 is atomic like.

Figures 3 and 4 show that those harmonic peaks near the cutoff regime are structureless. However, for harmonics in the plateau and well below the cutoff, they possess some multiple-peak fine structures. As shown in our recent time-frequency analysis of the HHG power spectrum of atomic H [42], these fine structures carry significant information regarding detailed HHG mechanisms.

To explore the detailed spectral and temporal structure of HHG and the underlying mechanisms in different energy regimes, we perform the time-frequency analysis by means of

TABLE I. The comparison of the length and acceleration forms of HHG power spectra of H_2. The laser wavelength and intensity used are, respectively, 1064 nm and 10^{14} W/cm^2. (HO stands for "harmonic order.") The internuclear distance is fixed at $R=1.4$ a.u.

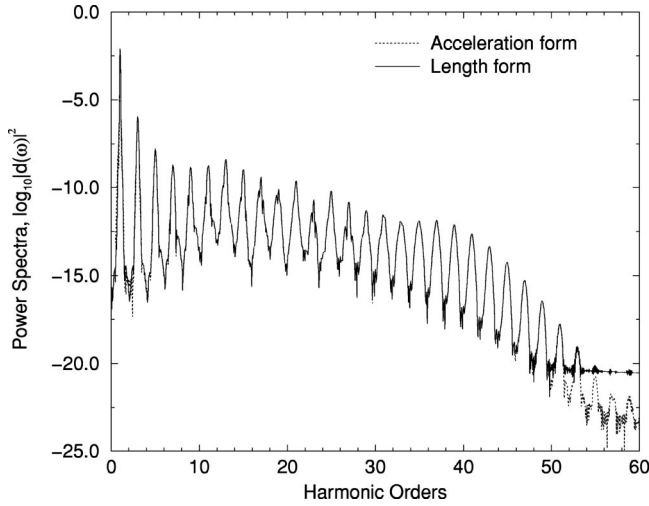| HO	Length form	Acceleration form	HO	Length form	Acceleration form
3	-5.99	-5.97	27	-10.81	-10.81
5	-7.75	-7.77	29	-11.32	-11.35
7	-8.73	-8.71	31	-11.70	-11.69
9	-8.84	-8.84	33	-12.07	-12.04
11	-8.75	-8.75	35	-11.90	-11.89
13	-8.39	-8.39	37	-11.87	-11.88
15	-8.95	-8.95	39	-12.13	-12.14
17	-9.43	-9.43	41	-12.64	-12.65
19	-10.13	-10.12	43	-13.36	-13.36
21	-9.61	-9.62	45	-14.25	-14.26
23	-10.70	-10.70	47	-15.29	-15.30
25	-10.20	-10.19	49	-16.48	-16.50

FIG. 3. The HHG power spectrum of H_2 (at $R = 1.4a_0$) in a 20-optical cycle, 1064 nm, $\sin^2$ pulse shape laser fields with peak intensity 10^{14} W/cm^2. Both the length form (solid line) and acceleration form (dotted line) power spectra are shown for comparison.

the wavelet transform [42,43] of the induced dipole (or dipole acceleration),

$$A_W(t_0, \omega) = \int d(t) W_{t_0, \omega}(t) dt \equiv d_\omega(t), \qquad (44)$$

with the wavelet kernel $W_{t_0, \omega}(t) = \sqrt{\omega} W(\omega(t - t_0))$. For the harmonic emission, a natural choice of the mother wavelet is given by the Morlet wavelet [43]

$$W(x) = (1/\sqrt{\tau}) e^{ix} e^{-x^2/2\tau^2}. \qquad (45)$$

Unlike the Garbor transform [43] where the width of the window function is fixed, the wavelet window function varies with the frequency but the total number of oscillations (proportional to τ) within the window is held constant. We have tested the dependence of $d_\omega(t)$ on the parameter τ by
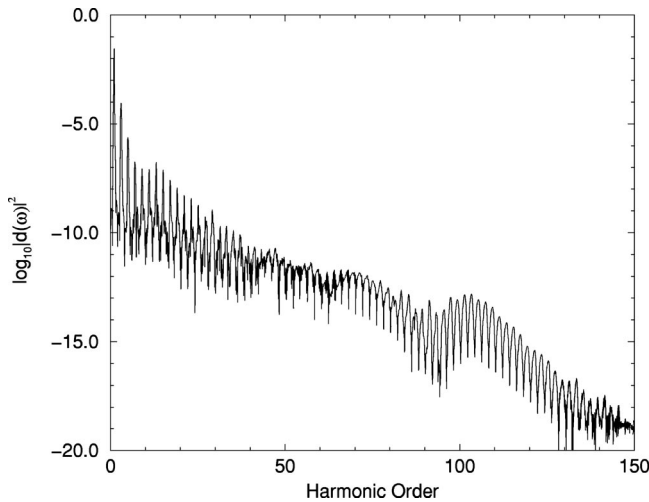

FIG. 4. The HHG power spectrum of H_2 ($R = 1.4a_0$) in a 20-optical cycle, 1064 nm, $\sin^2$ pulse shape laser fields with peak intensity 3×10^{14} W/cm^2.

varying its value from 5 to 30. Although the absolute value of $d_\omega(t)$ changes a little, the general pattern does not change. In the discussion below we choose $\tau = 15$ to perform the wavelet transform. We found the time profiles obtained by the induced dipole and acceleration are essentially identical, indicating the full convergence of the time-dependent results.

Figure 5 shows the modulus of the time-frequency profiles of H_2 (at $R = 1.4a_0$) in (1064 nm, 20 o.c., $\sin^2$ pulse shape, and 10^{14} W/cm^2) laser fields, revealing striking and vivid details of the spectral and temporal structures. Figures 6(a)–6(d) show representative time profiles of harmonics in different energy regimes obtained by performing the cross section of the time-frequency profile in Fig. 5 at a given harmonic frequency. Several salient features are noticed. (a) First, for the lowest few harmonics, the time profile (at a given frequency) shows a smooth function of the driving laser pulse. This is an indication that the multiphoton mechanism dominates this lower harmonic regime. In this regime, the probability of absorbing N photons is roughly proportional to I^N, and I (laser intensity) is proportional to $E(t)^2$. (b) Second, the smooth time profile is getting shorter (in time duration) and broadened (in frequency) as the harmonic order is increased, as is evident in Fig. 5 and Fig. 6(a) from the 1st to the 7th harmonics. As the harmonic order is further increased, the time profiles (see particularly the 11th harmonic in Fig. 5) develop extended fine structures. This can be attributed to the effect of excited states and the onset of the ionization threshold. (c) Third, for those high harmonics in the plateau regime well above the ionization threshold, the most prominent feature is the development of fast burst time profiles. At a given time, we see that such bursts actually form a *continuous frequency profile* in Fig. 5. This is clear evidence of the existence of the bremsstrahlung radiation emitted by each recollision of the electron wave packet with the parent ionic core(s). This confirms the bremsstrahlung model of HHG [45]. In contrast, we find that the (multiphoton-dominant) lowest-order harmonics form a *continuous time profile* at a given frequency. In the intermediate energy regime, where both multiphoton and tunneling mechanisms contribute, the time-frequency profiles show a netlike structure, as seen in Fig. 5.

Now we focus on the discussion of the origin of the power spectrum patterns near and below the cutoff in Fig. 3. Figures 7 and 8 show, respectively, the time profiles of 43th and 23th harmonics obtained by performing the cross section of the time-frequency profile of Fig. 5 at a given harmonic frequency. Figure 7 shows a representative time profile near the cutoff, which exhibits two bursts within each optical cycle. Each burst is due to the recollision of the electronic wave packet with the ionic core(s). Although H_2 has two ionic centers, a quasiclassical analysis of two-center systems [44] shows that the the two-center effect is not appreciable at short internuclear distance such as that at $R_e = 1.4a_0$, the present focus. Thus the pattern seen in Fig. 7 is atomiclike. However, the classical returning times (indicated by the vertical-dotted lines in Fig. 7) do not coincide with our quantum prediction of the light-emission times. This indicates that the electron-nuclear interactions (which are ignored in the quasiclassical model) are significant in the determination
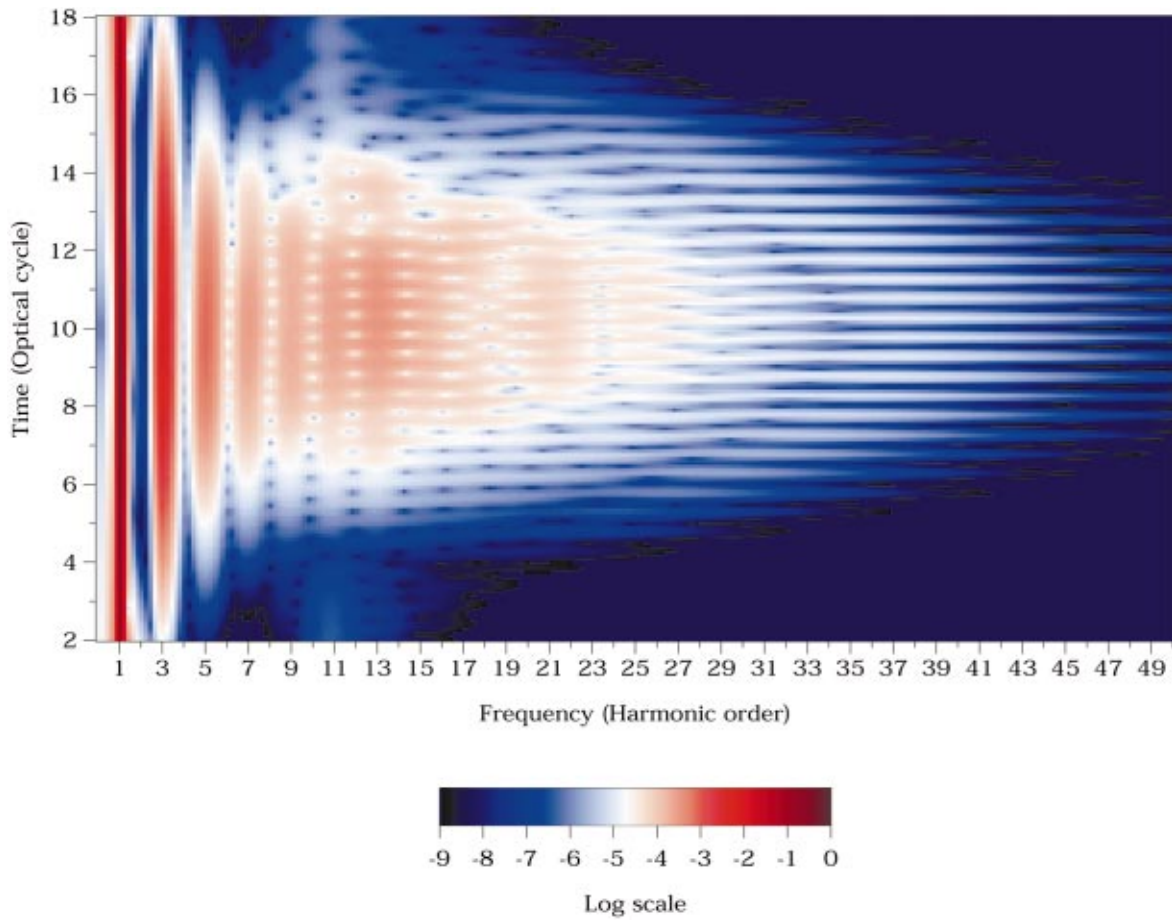
FIG. 5. (Color) The time-frequency spectra (modulus) of H_2 (at $R = 1.4a_0$) in (1064 nm, 20 o.c., $\sin^2$ pulse shape) laser fields with peak intensity 10^{14} w/cm^2. The colors shown are in logarithmic scale (in powers of 10).
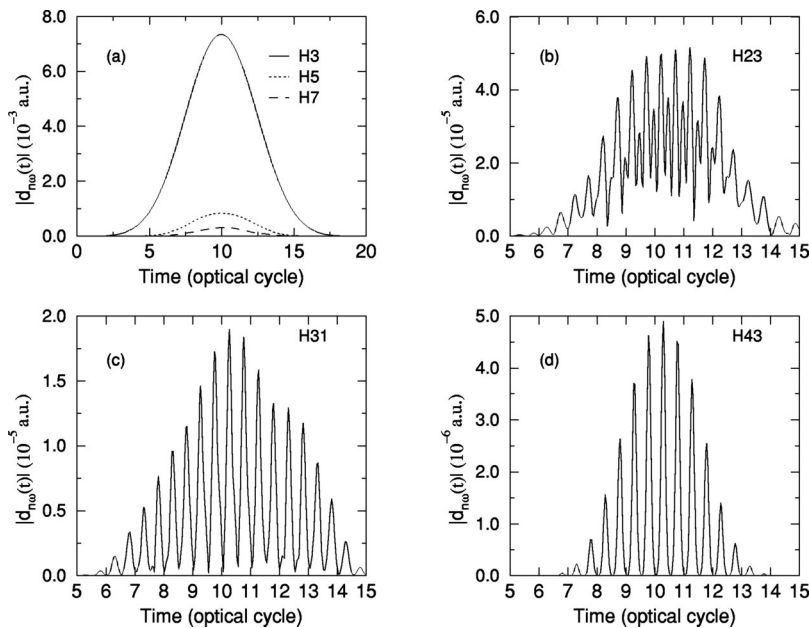

FIG. 6. The time profiles of *nth* harmonics of H_2 ($R = 1.4a_0$) in different energy regimes. The laser parameters are the same as those in Fig. 3.
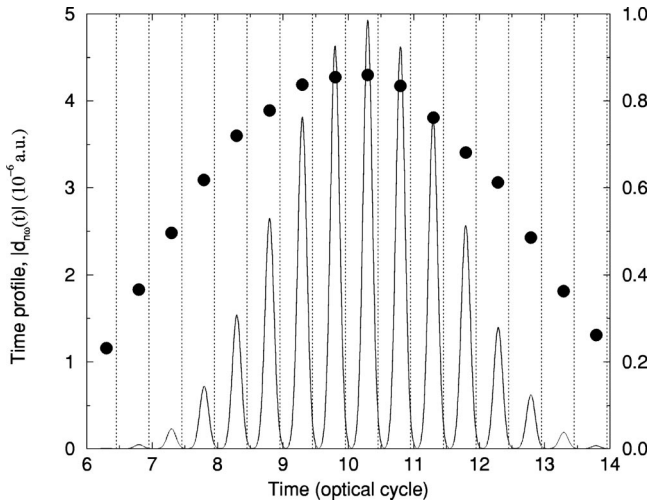
FIG. 7. The time profile of the 43rd (near cutoff) harmonic of H_2. The laser parameters are the same as those in Fig. 3. Also shown here are the dynamical phases (black dots) and classical returning times (vertical-dotted lines).

FIG. 9. The time profiles of the subpeaks of the 23rd harmonic of H_2 ($R = 1.4a_0$) in intense pulsed laser fields. The laser parameters are the same as those in Fig. 3.

of the actual harmonic time-frequency profiles. As the laser intensity is increased, however, we find that the classical returning times are actually getting closer to the quantal prediction for near cutoff harmonics (not shown). This is consistent with the fact that as the laser interaction becomes more dominant than the Coulomb potential, the quasiclassical model for cutoff harmonics become more valid.

Next we consider the time-frequency behavior of those harmonics below the cutoff. According to the quantum model (in the strong-field approximation) for one-center systems [46,47], when the electron return energy is below the cutoff, there exists two returning trajectories: the first (''short'') trajectory returns at a phase (ωt) less than 342 ° (or 162 °), and the second (''long'') trajectory at a phase larger than 342 ° (or 162 °). This feature is confirmed in Fig. 8, where we show a representative time profile for harmonics
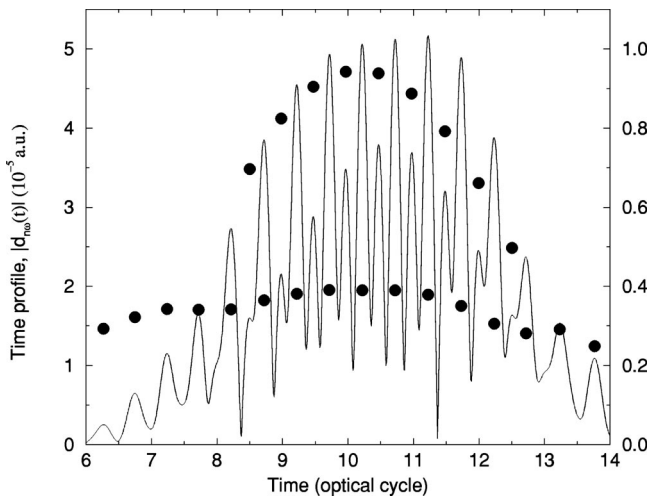

FIG. 8. The time profiles of the 23rd harmonic (below cutoff) of H_2. The laser parameters are the same as those in Fig. 3. The dynamical phases are shown as black dots.
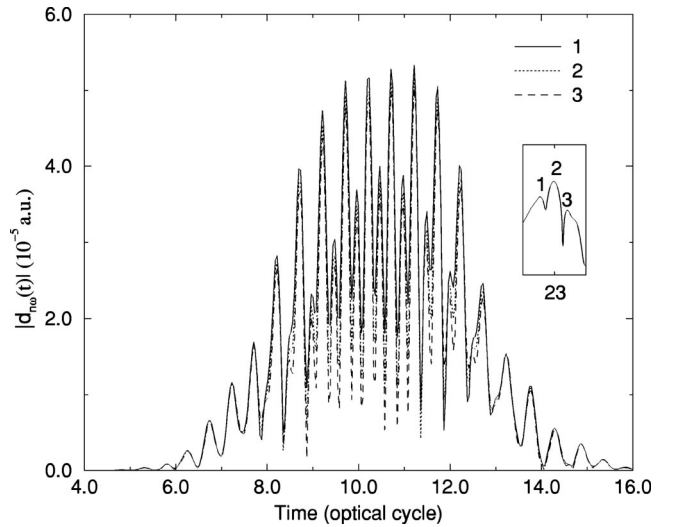
in the plateau below the cutoff. In this case, there exists two bursts of light emission for each half optical cycle for the time range corresponding to the central part of the laser pulse.

Also shown in Figs. 7 and 8 are the ''dynamical phases'' $\theta(t_q)$ (denoted by black dots) obtained from the wavelet transform of the induced dipole (or dipole acceleration), corresponding to each instant (t_q) of electron-ion core recollision:

$$d_\omega(t_q) = |d_\omega(t_q)| e^{-iS(t_q)}, \qquad (46)$$

where $S(t_q) = \omega t_q + \theta(t_q)$. First we note that the dynamical phase for the harmonics near the cutoff, Fig. 7, show a time profile mimic the laser-pulse shape. For the harmonics below the cutoff, we see in Fig. 8 that the ''long'' electronic trajectory has stronger phase dependence on laser intensity than that of ''short'' one. Similar feature was observed in our recent *ab initio* quantum study of the atomic H systems [42].

Finally it is instructive to explore the origin of the fine-structure peak splitting of harmonics in the plateau regime below the cutoff, see for example, the 23rd harmonic in Fig. 3. Figure 9 shows the time profiles at the three sub-peak positions (denoted by 1, 2, and 3) within the 23rd harmonic. Strikingly, their time profiles nearly coincide. This is an evidence that all the harmonic subpeaks within a given harmonic are produced by the same mechanism, namely, they are produced by the interference in time of all the bremsstrahlung radiation emitted from all the returning electronic wave packets within the incident laser-pulse duration. To our knowledge, this is the first *ab initio* calculation exhibiting the details of the time profiles of the subpeak harmonics for a molecular system.

In conclusion, we have presented the first TDDFT/OEP-SIC formalism for molecular systems and applied the proce-

dure for a detailed study of the HHG processes of H_2 (at equilibrium internuclear distance) in intense pulsed laser-fields. We have also explored the fine structure of HHG spectrum by means of the wavelet time-frequency transform. Our analysis provides new information and insights regarding the underlying HHG mechanisms in different energy regimes for the homonuclear diatomic systems for the first time. Extension of the present paper to include the nuclear vibrational degree of freedom and to the study of two-center

effect on molecular HHG at larger R will be considered in a future publication.

ACKNOWLEDGMENTS

[1] P. Hohenberg and W. Kohn, Phys. Rev. **136**, B864 (1964).

[2] W. Kohn and L. J. Sham, Phys. Rev. **140**, A1133 (1965).

[3] R. Parr and W. Yang, *Density-Function Theory of Atoms and Molecules* (Oxford University Press, New York, 1989).

[4] R. M. Dreizler and E. K. U. Gross, *Density Functional Theory, An Approach to the Quantum Many-Body Problem* (Springer-Verlag, Berlin, 1990).

[5] *Density Functional Theory*, Vol. 337 of *NATO Advanced Study Institute, Series B: Physics*, edited by E. K. U. Gross and R. M. Dreizler (Plenum, New York, 1995).

[6] N. H. March, *Electron Density Theory of Atoms and Molecules* (Academic, San Diego, 1992).

[7] *Density Functional Methods in Chemistry*, edited by J. K. Labanowski and J. W. Andzelm (Springer-Verlag, Berlin, 1991).

[8] E. Runge and E. K. U. Gross, Phys. Rev. Lett. **52**, 997 (1984).

[9] E. K. U. Gross and W. Kohn, Adv. Quantum Chem. **21**, 255 (1990).

[10] G. D. Mahan and K. R. Subbaswamy, *Local Density Theory of Polarizability* (Plenum Press, New York, 1990).

[11] C. A. Ullrich, U. J. Gossmann, and E. K. U. Gross, Phys. Rev. Lett. **74**, 872 (1995).

[12] X. M. Tong, and S. I. Chu, Phys. Rev. A **57**, 452 (1998).

[13] X. M. Tong and S. I. Chu, Int. J. Quantum Chem. **69**, 293 (1998).

[14] G. Vignale, C. A. Ullrich, and S. Conti, Phys. Rev. Lett. **79**, 4878 (1997).

[15] D. Telnov and S. I. Chu, Chem. Phys. Lett. **264**, 466 (1997).

[16] D. Telnov and S. I. Chu, Phys. Rev. A **58**, 4749 (1998).

[17] For reviews on generalized Floquet formalisms, see, S. I. Chu, Adv. At. Mol. Phys. **21**, 197 (1985); S. I. Chu, Adv. Chem. Phys. **73**, 739 (1989).

[18] S. J. Vosko, L. Wilk, and M. Nusair, Can. J. Phys. **58**, 1200 (1980).

[19] A. D. Becke, Phys. Rev. A **38**, 3098 (1988).

[20] C. Lee, W. Yang, and R. G. Parr, Phys. Rev. B **37**, 785 (1988).

[21] J. P. Perdew and Y. Wang, Phys. Rev. B **33**, 8800 (1986).

[22] X. M. Tong and S. I. Chu, Phys. Rev. A **55**, 3406 (1997).

[23] J. B. Krieger, Y. Li, and G. J. Iafrate, Phys. Lett. A **146**, 256 (1990).

[24] R. T. Sharp and G. K. Horton, Phys. Rev. **90**, 317 (1953).

[25] J. D. Talman and W. F. Shadwick, Phys. Rev. A **14**, 36 (1976).

[26] J. P. Perdew and A. Zunger, Phys. Rev. B **23**, 5048 (1981).

[27] See, for example, G. Yao and S. I. Chu, Chem. Phys. Lett. **197**, 413 (1992); J. Wang and S. I. Chu, *ibid.* **227**, 663 (1994).

[28] C. Canuto, M. Y. Hussaini, A. Quarteroni, and T. A. Zang, *Spectral Methods in Fluid Dynamics* (Springer-Verlag, Berlin, 1988).

[29] M. R. Hermann and J. A. Fleck Jr., Phys. Rev. A **38**, 6000 (1988).

[30] T. F. Jiang and S. I. Chu, Phys. Rev. A **46**, 7322 (1992).

[31] K. C. Kulander, Phys. Rev. A **36**, 2726 (1987).

[32] C. A. Ullrich and E. K. U. Gross, Comments At. Mol. Phys. **33**, 211 (1997).

[33] For a recent review of HHG, see P. Salieres, A. L'Huillier, Ph. Antoine, and M. Lewenstein, Adv. At., Mol., Opt. Phys. **41**, 83 (1999).

[34] X. M. Tong and S. I. Chu, Chem. Phys. **217**, 119 (1997).

[35] D. E. Ramaker and J. M. Peek, At. Data **5**, 167 (1973).

[36] W. Kolos and L. Wolniewicz, J. Chem. Phys. **105**, 213 (1996).

[37] P. B. Corkum, Phys. Rev. Lett. **71**, 1994 (1993).

[38] K. C. Kulander *et al.*, in *Super-Intense Laser-Atom Physics*, Vol. 316 of NATO *Advanced Study Institute Series B: Physics*, edited by P. B. Piraux *et al.* (Plenum, New York, 1993).

[39] S. C. Rae, K. Burnett, and J. Cooper, Phys. Rev. A **50**, 3438 (1994).

[40] D. Normand, L. A. Lompre, and C. Cornaggia, J. Phys. B **25**, L497 (1992).

[41] B. Friedrich and D. Herschbach, Phys. Rev. Lett. **74**, 4623 (1995).

[42] X. M. Tong and S. I. Chu, Phys. Rev. A **61**, 021802 (2000).

[43] C. K. Chui, *An Introduction to Wavelets* (Academic Press, New York, 1992).

[44] (a) X. Chu (unpublished); (b) R. Kopold *et al.*, Phys. Rev. A **58**, 4022 (1998).

[45] M. Protopapas *et al.*, Phys. Rev. A **53**, R2933 (1996).

[46] M. Lewenstein *et al.*, Phys. Rev. A **49**, 2117 (1994).

[47] C. Kan *et al.*, Phys. Rev. A **52**, R4336 (1995).